Biomaterials 35 (2014) 4255–4265

Contents lists available at ScienceDirect

Biomaterials

journal homepage: www.elsevier.com/locate/biomaterials

Antibacterial effects and biocompatibility of titanium surfaces with graded silver incorporation in titania nanotubes

Shenglin Mei [a,b,d,1], Huaiyu Wang [b,c,1], Wei Wang [a], Liping Tong [b], Haobo Pan [c], Changshun Ruan [c], Qianli Ma [a], Mengyuan Liu [a], Huiling Yang [a], Liang Zhang [a], Yicheng Cheng [a], Yumei Zhang [a,*], Lingzhou Zhao [a,*], Paul K. Chu [b,*]

[a] School of Stomatology, The Fourth Military Medical University, Xi'an 710032, China
[b] Department of Physics & Materials Science, City University of Hong Kong, Tat Chee Avenue, Kowloon, Hong Kong, China
[c] Center for Human Tissues and Organs Degeneration, Shenzhen Institutes of Advanced Technology, Chinese Academy of Sciences, Shenzhen 518055, China
[d] Department of Stomatology, The 518th Military Hospital, Xi'an 710043, China

ARTICLE INFO

Article history:
Received 18 December 2013
Accepted 4 February 2014
Available online 22 February 2014

Keywords:
Titania nanotubes
Silver
Plasma immersion ion implantation
Antibacterial effects
Biocompatibility

ABSTRACT

Most commercial dental implants are made of titanium (Ti) because Ti possesses excellent properties such as osseointegration. However, many types of Ti products still suffer from insufficient antibacterial capability and bacterial infection after surgery remains one of the most common and intractable complications. In this study, a dual process encompassing anodization and silver plasma immersion ion implantation (Ag PIII) is utilized to produce titania nanotubes (TiO_2-NTs) containing Ag at different sites and depths. The concentration and depth of the incorporated Ag can be tailored readily by changing the PIII parameters. The Ag-embedded TiO_2-NTs which retain the nanotubular morphology are capable of sterilizing oral pathogens as opposed to pure Ti plates and pristine TiO_2-NTs. Biological assays indicate that the *in vitro* and *in vivo* biocompatibility of the sample plasma-implanted at a lower voltage of 0.5 kV (NT-Ag-0.5) is significantly compromised due to the large amount of surface Ag. On the other hand, the sample implanted at 1 kV (NT-Ag-1.0) exhibits unimpaired effects due to the smaller surface Ag accumulation. Sample NT-Ag-1.0 is further demonstrated to possess sustained antibacterial properties due to the large embedded depth of Ag and the technique and resulting materials have large potential in dental implants.

1. Introduction

Titanium (Ti) and Ti alloys which have good mechanical properties, high corrosion resistance, excellent biocompatibility [1,2] are commonly found in orthopedic prostheses, orthodontics, joint replacements, and so on [1,3–5]. Although Ti products account for a large proportion of the commercial dental market, their antibacterial properties are inadequate in many applications and despite thorough disinfection in advance, microbial infection remains one of the intractable problems [6,7]. Microorganisms are abundant in the oral environment and the trans-gingival abutment of the implants is an important portal for bacterial infection [8]. The surgical trauma after implantation can also compromise the host defense consequently facilitating bacterial invasion. Implant failure can be a direct consequence of serious microbial attack and hence, new Ti-based biomaterials with the desirable antibacterial properties are essential for high quality dental care.

There have been studies about incorporating antibacterial agents into the surface of biomedical implants [9–12]. However, most of these attempts fail to deliver sustained antibacterial effects as the surface layers and coatings are prone to rapid degradation in the oral environment. In fact, fast release of antibacterial agents causes safety concerns and the emergence of resistant strains is another issue when excessive antibiotics are administered [8]. In contrast to antibiotics, silver (Ag) is a non-specific bactericide that acts against a broad spectrum of bacterial and fungal species. Ag is attractive on account of the good stability in the physiological environment and the difficulty to develop resistant strains [6–8,13–16], although it has been documented that the therapeutic window of Ag is rather small [17,18] and Ag is cytotoxic above a certain dose. Nevertheless,

* Corresponding authors.
E-mail addresses: wqtzym@fmmu.edu.cn (Y. Zhang), zhaolingzhou1983@hotmail.com (L. Zhao), paul.chu@cityu.edu.hk (P.K. Chu).
[1] These 2 authors contributed equally to this work.

http://dx.doi.org/10.1016/j.biomaterials.2014.02.005
0142-9612/

by introducing the proper amount of Ag into the implants and controlling its release, excellent antibacterial properties can be attained without compromising the original biological functions of the substrate [14–16].

Titania nanotubes (TiO_2-NTs) have attracted much attention due to their low elastic modulus [19] and unique topography [20–22]. The dimensions of TiO_2-NTs can be controlled and TiO_2-NTs with certain dimensions do not impair and even promote the biological properties of the Ti substrate [20–22]. Furthermore, the "half-open" structure of TiO_2-NTs can serve as the reservoir to store antibacterial agents such as Ag [7,23] to produce sustained antibacterial effects. In this study, TiO_2-NTs are fabricated on Ti by anodization and low-voltage Ag plasma immersion ion implantation (PIII) is conducted to embed Ag at different depths without breaking the nanotubular structure. The different antibacterial characteristics rendered by the different Ag depth distributions and subsequent biocompatibility are assessed systematically both *in vitro* and *in vivo*.

2. Materials and methods

2.1. Sample preparation

Commercial pure Ti plates (10 mm × 10 mm × 1 mm) were polished and ultrasonically cleaned in acetone, ethanol, and deionized water. Table 1 lists the different processing parameters together with sample designations. PT denotes the untreated pure Ti as the control. Sample NT underwent anodization at a constant voltage of 20 V for 30 min [24] and samples NT-Ag-0.5 and NT-Ag-1.0 were subjected to Ag PIII at different voltages. Ag PIII was conducted on a plasma ion implanter equipped with a filtered cathodic arc plasma source made of 99.99% pure Ag. A curved magnetic duct was inserted between the plasma source and main chamber to remove macro-particles produced from the cathodic arc [16] and during Ag PIII, the pulse of cathodic arc was synchronized with that of the target voltage.

2.2. Surface characterization

Scanning electron microscopy (SEM, S-4800, Hitachi High Technologies) and atomic force microscopy (AFM, NanoScope V MultiMode system, Veeco) were employed to evaluate the surface morphology. The samples were dried and sputter-coated with platinum prior to SEM examination and the surface roughness was determined by AFM. X-ray photoelectron spectroscopy (XPS) was conducted on a Physical Electronics PHI 5802 equipped with a monochromatic Al K_α source. A constant pass energy (11.75 eV) was employed and all the data were collected at a take-off angle of 45°. The static contact angles were measured by the static sessile drop method on the EasyDrop Standard instrument (KRUSS) at ambient humidity and temperature. Distilled water, formamide, and diiodomethane were used as the media (10 μl per drop) and 6 measurements were performed on each specimen for statistical accountability.

2.3. Bacteria culture

Porphyromonas gingivalis (Pg, ATCC33277) and *Actinobacillus actinomycetemcomitans* (Aa, ATCC29523) were cultivated in the brain heart infusion (BHI, Oxoid) broth medium supplemented with blood. Both kinds of bacteria were involved in the assays of various samples. The specimens were placed on 24-well culture plates and separately incubated in 1 ml of the bacteria-containing medium (10^6 CFU ml^{-1}) under standard anaerobic conditions (80% N_2, 10% H_2, 10% CO_2, at 37 °C) [25] for different time durations. Before bacteria incubation, the substrates were sterilized with 75% alcohol overnight and rinsed three times with a sterile phosphate buffered saline (PBS) solution.

2.3.1. Fluorescence staining

After exposure to bacteria for 1 day, the specimens were rinsed three times with PBS, stained with SYTO 9 and propidium iodide dyes (LIVE/DEAD® BacLight™ Bacterial Viability Kits, Molecular Probes) for 15 min in darkness, and examined by laser scanning confocal microscopy (FV1000, Olympus). The fluorescence intensity was monitored by the Olympus software kit (OLYMPUS FLUOVIEW Ver.3.1 Viewer).

2.3.2. SEM observation

After bacteria incubation for 1 day, the substrates were rinsed thrice with PBS, fixed with 3% glutaraldehyde at 4 °C for 2 h, and dehydrated sequentially in a series of ethanol solutions for 10 min each. Prior to SEM observation, the specimens were dried and sputter coated with platinum.

2.3.3. Antibacterial assay

After culturing for 1, 4, and 7 days, the bacteria on the various specimens were gently rinsed with PBS and ultrasonically detached in 1 ml of the PBS solution for 5 min. The bacteria suspensions were re-cultivated on agar plates for colony counting. The antibacterial rates were determined by the following relationship: Antibacterial rate (%) = (CFU of control − CFU of experimental groups)/CFU of control × 100%, where PT served as the control and NT, NT-Ag-0.5, and NT-Ag-1.0 constituted the experimental groups.

2.4. Ag release test

The 28-day Ag release from NT-Ag-0.5 and NT-Ag-1.0 was monitored in 5 ml of PBS solution at 37 °C under agitation (60 revolutions per minute) and periodic replacements of the PBS. The Ag^+ concentration of each harvested specimen was quantitatively determined by inductively-coupled plasma mass spectrometry (ICP-MS, Thermo X series 2).

2.5. Cell culture

Both the epithelia-like cell line Tca-8113 and fibroblast-like cell line HT1080 were used. Tca-8113 and HT1080 were cultured in RPMI-1640 medium (Sigma) and Dulbecco's modified eagle medium (DMEM, Gibco) supplemented with 10% newborn bovine serum, respectively, in a humidified atmosphere of 5% CO_2 at 37 °C. The cells were seeded onto the specimens at a density of 2×10^4 cells per sample by using 24-well tissue culture plates as the holders. Before cell seeding, the substrates were sterilized with 75% alcohol overnight and rinsed three times with sterile PBS.

2.5.1. Cell viability assay

After incubation for 1, 4, and 7 days, the samples were rinsed three times with sterile PBS and incubated with a 1 mg/mL 3-(4,5-dimethylthiazol-2-yl)-2,5-diphenyltetrazolium bromide (MTT, Sigma) solution at 37 °C for 4 h to allow formazan formation. The formazan was dissolved by dimethyl sulfoxide and the optical density (OD) was determined spectrophotometrically at 570 nm.

2.5.2. Morphological determination

After culturing for 1 day, the substrates were rinsed three times with PBS, fixed with 3% glutaraldehyde at 4 °C for 2 h, and dehydrated in a series of ethanol solutions for 10 min each. The dehydrated samples were dried, platinum coated, and examined by SEM.

2.5.3. Real-time polymerase chain reaction (RT-PCR)

After culturing with cells for 7 days, the specimens were rinsed three times with PBS, and the total RNA of the cultured cells was extracted by a TRIZOL reagent (Invitrogen). One μg of RNA from each specimen was reverse transcribed into cDNA by a PrimeScript™ RT reagent kit (TaKaRa) according to the manufacturer's protocols. RT-PCR was performed on a Bio-Rad iQ5 real time PCR system using a mixture of SYBR® Premix Ex Taq II (TaKaRa), cDNA templates, and the primers. Vascular endothelial growth factor (VEGF) and fibronectin (FN) of the cultured epithelial cells, and type I collagen (Coll-I) and intercellular adhesion molecule-1 (ICAM-1) of the cultured fibroblasts were analyzed with glyceraldehyde-3-phosphate dehydrogenase (GAPDH) serving as an endogenous house-keeping gene for normalization. The primer sequences of the genes are shown in Table 2. Quantification of the gene expressions was based on the comparative cycle-threshold method.

2.6. Animals and surgery

The animal experiments were approved by Institutional Animal Care and Use Committee of the Fourth Military Medical University, and a total of 12 male Sprague-Dawley rats (weighing 200–250 g) were used. The animals were housed under a

Table 1
Main parameters of the anodization and plasma immersion ion implantation processes.

Sample name	Anodization		Ag plasma immersion ion implantation				
	Voltage (V)	Treatment time (min)	Pulse duration (μs)	Pulse frequency (Hz)	Pressure (Pa)	Treatment time (min)	Voltage (kV)
PT	–	–	–	–	–	–	–
NT	20	30	–	–	–	–	–
NT-Ag-0.5	20	30	3000	10	1.8×10^{-4}	90	−0.5
NT-Ag-1.0	20	30	3000	10	1.8×10^{-4}	90	−1.0

Table 2
Sequences of the primers for cell RT-PCR.

Gene	Primers
VEGF	5′-GAGCCTTGCCTTGCTGCTCTAC-3′
	5′-CACCAGGGTCTCGATTGGATG-3′
FN	5′-ACCTACGGATGACTCGTGCTTTGA-3′
	5′-CAAAGCCTAAGCACTGGCACAACA-3′
Coll-I	5′-TCTAGACATGTTCAGCTTTGTGGAC-3′
	5′-TCTGTACGCAGGTGATTGGTG-3′
ICAM-1	5′-TGAGCAATGTGCAAGAAGATAGC-3′
	5′-CCCGTTCTGGAGTCCAGTACA-3′
GAPDH	5′-GCACCGTCAAGGCTGAGAAC-3′
	5′-TGGTGAAGACGCCAGTGGA-3′

12 h light/dark cycle with free access to water and food. Prior to surgery, the rats were anesthetized by inhaling 1.25–2.5% isoflurane with 100% oxygen. Thereafter, 2 parallel incisions (8 mm long) were made through the shaved and cleaned back skin of each rat, and then 4 small openings in the muscle sheath were made by dissection on both sides of the spine. All 4 types of samples were inserted into each rat and the implants were placed randomly in the openings with the modified surface placed toward the muscle tissue. The surgical wounds were closed with two sutures to secure the position of each implant. After surgery, the animals received intramuscular injections of gentamicin (2×10^5 U) to avoid postoperation infection.

2.6.1. Morphometry

At 12 days after implantation, the rats were sacrificed by an overdose of pentobarbital and the implants with the surrounding tissue attached were removed *en bloc*. After rinsing thrice in PBS, frozen at −80 °C, and immersing in 4% paraformaldehyde for 24 h, the specimens were dehydrated in a series of ethanol and embedded in paraffin. The embedded tissue was sectioned (6 μm thick) and stained by hematoxylin and eosin for light microscopy (DMI6000B, Leica). The thickness of the fibrotic capsule around each implant was determined at five equally located points on the side of modified surface for statistical accountability.

2.6.2. Immunohistochemistry

At 12 days after implantation, the rats were sacrificed and the tissue section (6 μm thick) of each implant was prepared following the above procedures. For macrophages staining, non-specific binding was initially removed by incubation in goal serum for 30 min and the sections were incubated with the mouse anti-rat cd68 monoclonal antibody (AbD Serotec) at 4 °C for 12 h. After three washes with PBS, the biotinylated secondary antibody (goal anti-mouse IG-FITC) was added and the sections were incubated at room temperature for 2 h in darkness. The specimens were washed thrice with PBS, counterstained by 4′,6-diamidino-2-phenylindol (DAPI), and mounted on slides for confocal microscopy (FV1000, Olympus). An Image-Pro Plus 6.0 software was utilized to determine the ratio of cd68-positive cells to total cells in each fibrotic capsule.

2.7. Statistics

The *in vitro* assays were performed in triplicate and values were expressed as mean ± standard deviation. Each *in vitro* experiment was repeated three times with data from a typical experiment shown. Six animals were involved in each *in vivo* assay with the data expressed as mean ± standard deviation. A one-way ANOVA combined with a Student-Newman-Keuls (SNK) *post hoc* test was utilized to determine the level of significance. In all the statistical evaluations, $p < 0.05$ was considered significant and $p < 0.01$ was considered highly significant.

3. Results

3.1. Surface characterization

The control, as-anodized, anodized and Ag PIII at 0.5 kV, and anodized and Ag PIII at 1 kV samples are designated as PT, NT, NT-Ag-0.5, and NT-Ag-1.0, respectively (Table 1). As shown in the SEM images in Fig. 1a, the typical nanotube array structure has a diameter of 80 nm and length of 270 nm. After Ag PIII at 0.5 and 1.0 kV, the nanotubular structure is preserved although the features are different. Ag is randomly deposited on the surface of NT-Ag-0.5 (Fig. 1b) but is found mainly on the inner nanotube wall of NT-Ag-1.0 (Fig. 1c). As a result, the nanotubular morphology of NT-Ag-0.5 is more obscure and the tube thickness of NT-Ag-1.0 increases. The 3-dimensional AFM images acquired from an area of 2.0 μm × 2.0 μm are displayed in Fig. 1d–g. In contrast to PT which has a planar microtopography, the samples after anodization are more rugged and the size of the granular structures (Fig. 1e–g) follows the following order: NT-Ag-0.5 > NT-Ag-1.0 > NT. The results are consistent with the SEM images that Ag is deposited randomly on NT-Ag-0.5 but mainly on the inner nanotube wall of NT-Ag-1.0. The sample surface roughness is also evaluated by AFM and the results are shown in Table 3. The roughness depends on the size of the granular structures and has the same order of NT-Ag-0.5 > NT-Ag-1.0 > NT. The difference in roughness originates from the absence as well as different locations of Ag.

XPS is performed to determine the Ag chemical states and depth profiles. As shown in Fig. 1h and i, the Ag3d peaks (368.25 eV and 374.25 eV) do not shift with depths and can be assigned to $3d_{5/2}$ and $3d_{3/2}$ of metallic Ag^0, indicating that the embedded Ag has the metallic (Ag^0) state. Ag is mainly located in the top 20 nm (about 76 at%) in NT-Ag-0.5 and the concentration diminishes rapidly to about 5 at% at a depth of 50 nm and less than 1 at% beyond 100 nm (Fig. 1h and j). On the other hand, the Ag concentration in NT-Ag-1.0 is 27 at% at 20 nm and decreases slowly with depth (Fig. 1i and j). Ag is detected from NT-Ag-1.0 throughout the entire nanotube length (270 nm). XPS, SEM, and AFM furnish evidence that Ag is incorporated at different depths without breaking the nanotubular structure. There is a larger amount of surface Ag on NT-Ag-0.5 than NT-Ag-1.0 but Ag penetrates more deeply in the latter sample.

The surface hydrophilicity affects bio-functions such as bacteria/cell adhesion and spreading. Here, it is evaluated by the static sessile drop method using distilled water, formamide and diiodomethane. As shown in Fig. 2, NT is more hydrophilic than PT, but Ag PIII undermines the surface hydrophilicity with the largest contact angles observed from NT-Ag-1.0. Among the 4 types of samples, only NT-Ag-1.0 is hydrophobic with a water contact angle >90° (Fig. 2).

3.2. Effects on oral pathogens

Dental implants are subjected to a variety of microbial strains in the oral environment, especially anaerobes and facultative anaerobes. In this study, two of these oral pathogens, Pg (Gram-positive bacteria) and Aa (Gram-negative bacteria) are utilized in the antibacterial evaluation. It has been documented that implants are most susceptible to surface bacteria colonization during the initial 6 h after implantation [26,27] and so the antimicrobial effects in the first day are critical to implant success. Fig. 3a depicts the representative images of re-cultivated bacteria after culturing for 1 day. The amounts of viable Pg and Aa on PT and NT are large, but those on NT-Ag-1.0 are few and those on NT-Ag-0.5 are even fewer. During the same time frame, the samples with bacteria incubation are evaluated by SYTO 9 and propidium iodide staining. The green-fluorescent SYTO 9 and red-fluorescent propidium iodide differ in their ability to penetrate bacterial cells. When both dyes are employed, the live bacteria with intact membranes fluoresce in green (stained by SYTO 9) and the dead bacteria with damaged membranes fluoresce in red (stained by propidium iodide). As shown in Fig. 3b, large amounts of live bacteria are detected from PT and NT. On the contrary, the vast majority of bacteria on NT-Ag-0.5 and NT-Ag-1.0 are dead as the viable bacteria that fluoresce in green are very few. The fluorescence intensities of the live, dead, and total (live and dead) bacteria are presented together in Table 4. In spite of the strongest sterilizing effect of NT-Ag-0.5, the smallest amount of total bacteria is observed from NT-Ag-1.0 instead of NT-Ag-0.5, possibly because the hydrophobic surface of NT-Ag-1.0 is less favorable to bacteria attachment.

SEM is performed to examine the morphology of the attached bacteria. Fig. 3c shows that Pg and Aa maintain their normal shape on PT and NT after incubation for 1 day. In the meantime, the

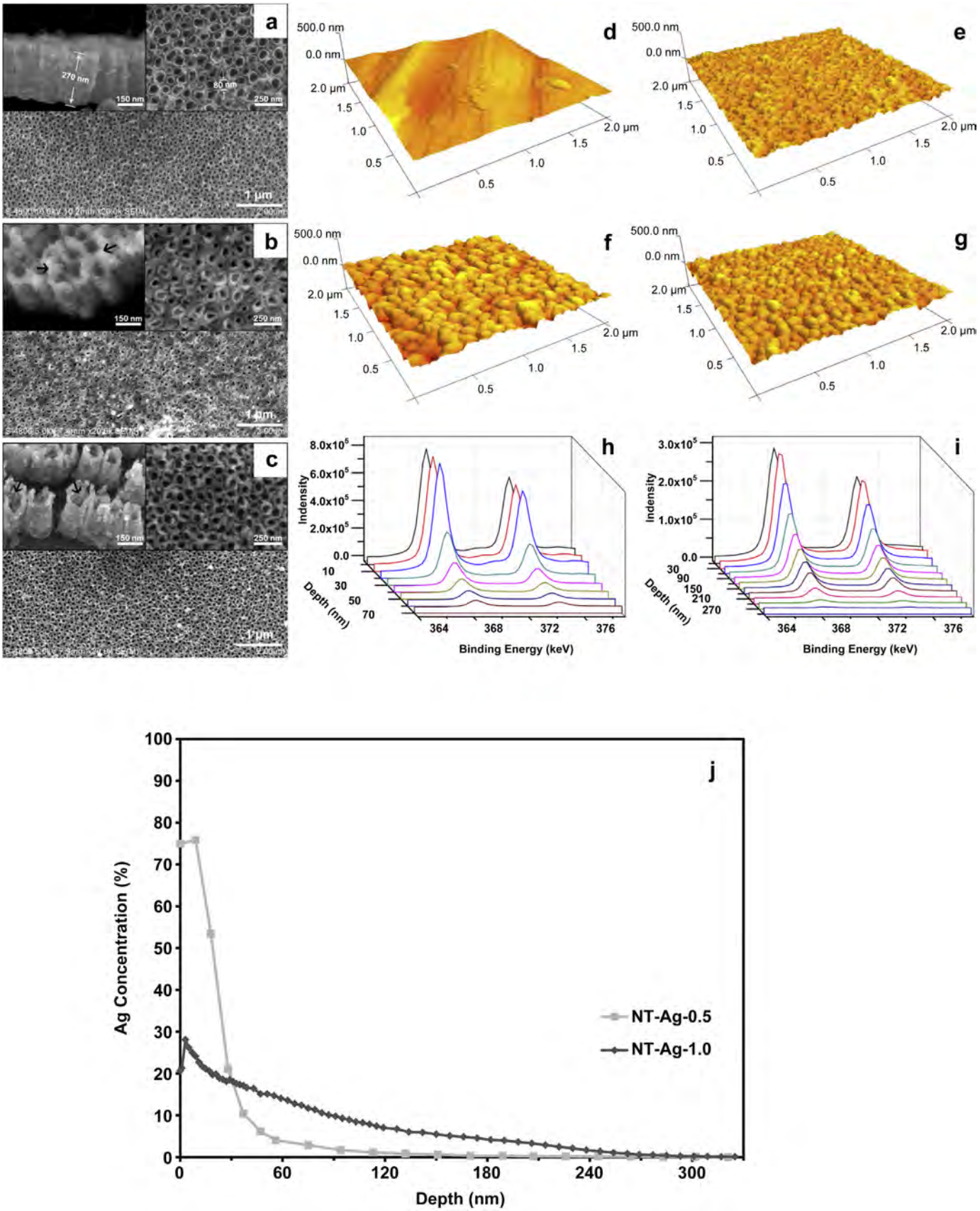

Fig. 1. Features of the samples characterized by SEM, AFM and XPS. (a–c) Top and oblique SEM observations of the samples designated as (a) NT, (b) NT-Ag-0.5 and (c) NT-Ag-1.0, black arrows referred to the introduced Ag. (d–g) 3-dimensional AFM images of (d) PT, (e) NT, (f) NT-Ag-0.5 and (g) NT-Ag-1.0, note the granular structures of NT, NT-Ag-0.5 and NT-Ag-1.0. (h, i) High-resolution Ag3d XPS spectra at different depths of (h) NT-Ag-0.5 and (i) NT-Ag-1.0, note the much deeper Ag impregnation of NT-Ag-1.0. (j) Ag depth profiles of NT-Ag-0.5 and NT-Ag-1.0.

Table 3
Surface roughness (mean ± SD) of the various samples determined by AFM. In the same column, values with different lowercase letter superscripts mean significant differences.

	R_a (nm)	R_q (nm)	R_z (nm)
PT	20.04 ± 2.25^a	25.18 ± 3.17^a	4.10 ± 0.25^a
NT	16.95 ± 1.86^b	21.40 ± 2.29^b	12.6 ± 1.95^b
NT-Ag-0.5	28.54 ± 3.34^c	35.33 ± 4.10^c	55.2 ± 6.84^c
NT-Ag-1.0	20.98 ± 2.61^a	26.59 ± 2.95^a	19.2 ± 2.12^b

adherent bacteria on NT-Ag-0.5 and NT-Ag-1.0 are rarely intact, indicating that most of these pathogens are inactivated. The seeded samples are further investigated by RT-PCR. The fimbrillin (encoding the distinct fimbriae of Pg, playing a key role in periodontal and peri-implant Pg invasion) [8,28] gene of Pg and cytolethal distending toxin B (a heat-labile protein cytotoxin produced by several Gram-negative bacteria including Aa, regulating the morphology of cultured bacteria) [29] gene of Aa are down-regulated by both NT-Ag-0.5 and NT-Ag-1.0 after 1 day (Fig. 4). The bactericidal activity of NT-Ag-0.5 and NT-Ag-1.0 is confirmed.

To monitor the sustained antibacterial effects, the bacteria incubation time is extended to 7 days. After different culturing time durations of 1, 4, and 7 days, the viable bacteria are detached from the samples and re-cultivated on agar plates to count the colonies. The antibacterial rates of NT, NT-Ag-0.5, and NT-Ag-1.0 are quantitatively referenced to PT and as shown in Fig. 5a and b, NT is better than PT in supporting bacterial survival. It is probably due to the nanotubular structure and excellent hydrophilicity of NT. On the other hand, NT-Ag-0.5 and NT-Ag-1.0 exhibit antibacterial effects to Pg and Aa, and NT-Ag-0.5 is more effective than NT-Ag-1.0 after 1 and 4 days. However, the antimicrobial activity of NT-Ag-0.5 decreases gradually with incubation time but that of NT-Ag-1.0 is nearly constant. Eventually, NT-Ag-1.0 is more antibacterial than NT-Ag-0.5 after 7 days.

As aforementioned, NT-Ag-0.5 and NT-Ag-1.0 are antibacterial but NT is not. The antimicrobial properties of NT-Ag-0.5 and NT-Ag-1.0 originate from the Ag introduced by PIII. It is generally accepted that the bactericidal activity of Ag-incorporated materials stems from leaching of Ag ions from the surface. NT-Ag-0.5 and NT-Ag-1.0 are separately immersed in a PBS solution and the concentration of leached Ag is determined by ICP-MS. The results in Fig. 5c indicate

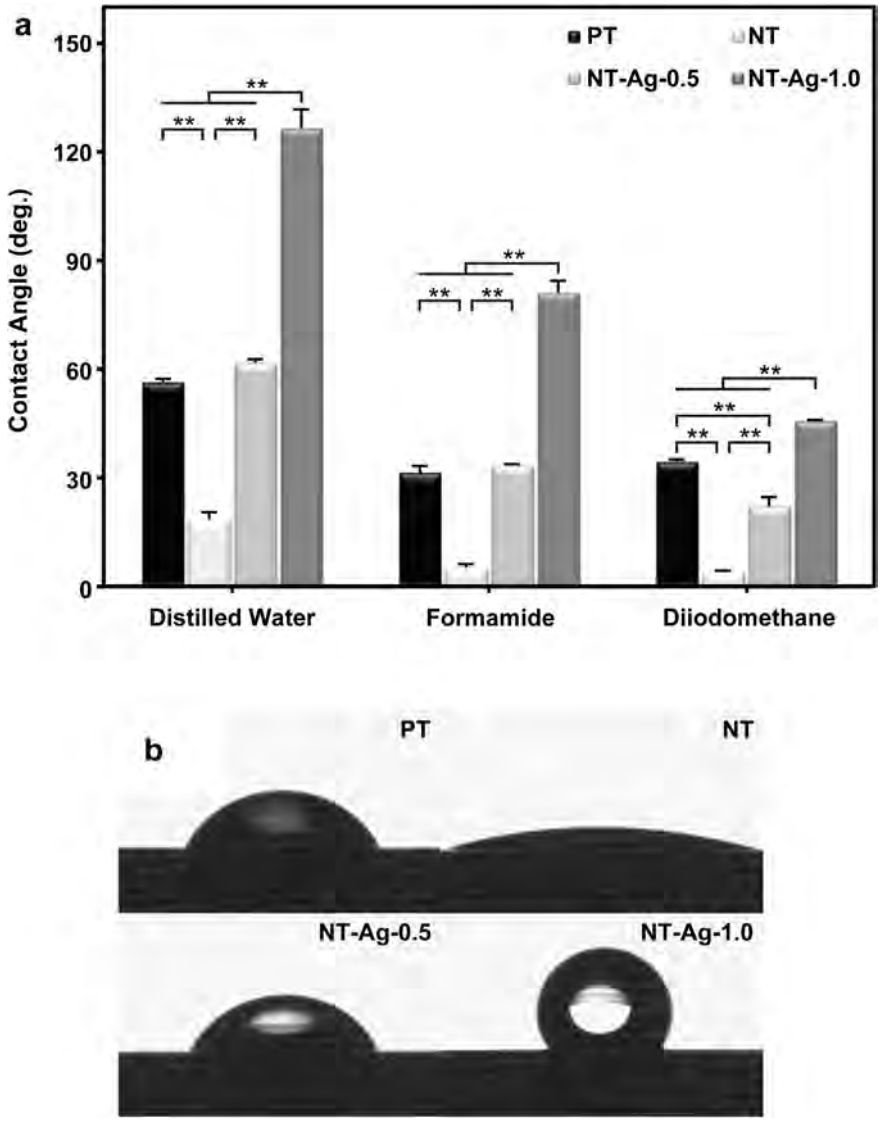

Fig. 2. (a) Water, formamide, and diiodomethane contact angles measured on various samples, note the excellent hydrophilicity of NT and the hydrophobicity of NT-Ag-1.0. One-way ANOVA followed by SNK post hoc test is utilized to determine the level of significance, $^{**}p < 0.01$. (b) Typical water droplet images on various samples.

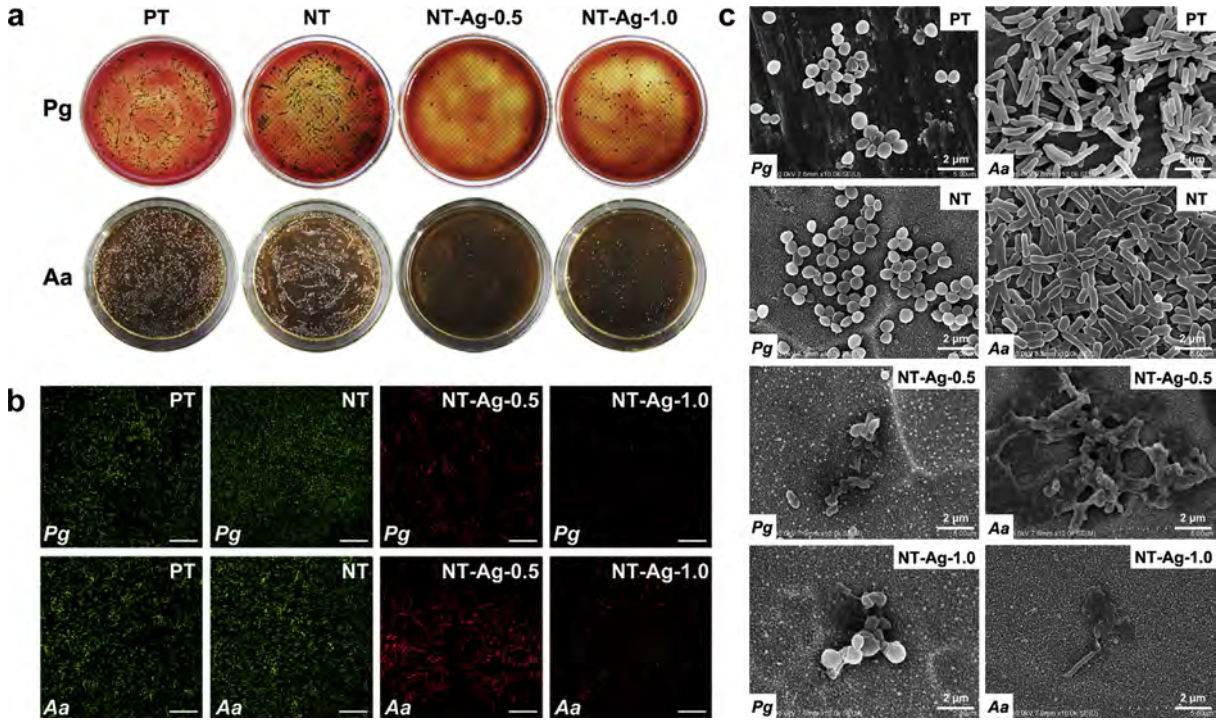

Fig. 3. Short-term bacteria incubation on the samples. (a) Typical images of re-cultivated Pg and Aa colonies from the samples after 1 day incubation, note that the re-cultivated bacteria colonies from PT and NT are numerous but those from NT-Ag-0.5 and NT-Ag-1.0 are scarce. (b) Confocal micrographs of bacteria cultured on various samples for 1 day with the green fluorescence referred to live bacteria and red fluorescence referred to dead bacteria and noting that the vast majority of bacteria on PT and NT are viable but those on NT-Ag-0.5 and NT-Ag-1.0 are inactivated. Scar bars for insets = 25 μm. (c) SEM images of bacteria on samples after incubation for 1 day noting that the bacteria on PT and NT have mainly the normal shape but those on NT-Ag-0.5 and NT-Ag-1.0 are rarely intact. (For interpretation of the references to color in this figure legend, the reader is referred to the web version of this article.)

that NT-Ag-0.5 is better than NT-Ag-1.0 initially. However, the cumulative Ag release from NT-Ag-1.0 rises faster with time. When the immersion time is 14 days or longer, the total Ag delivery from NT-Ag-1.0 is more dominant. In other words, although Ag release from NT-Ag-1.0 is not as substantial as that from NT-Ag-0.5 in the early stage, NT-Ag-1.0 fares better in terms of sustained Ag delivery.

3.3. *In vitro and in vivo evaluation*

The interactions between biomaterials and surrounding tissues are crucial to post-surgery recovery. With regard to dental implants, the trans-gingival parts face both epithelial and fibrous tissues and tight and healthy integration with these soft tissues is desirable. The samples are incubated with epithelial cells and fibroblasts to assess the roles in supporting cell functions. A colorimetric assay is first employed to measure the time-dependent viability of cells after 1, 4, and 7 days. As shown in Fig. 6a and b, NT is the most positive sample to both cell types whereas NT-Ag-0.5 is more unfavorable to the cells than PT. In spite of the hydrophobic surface which is generally considered to be negative to mammalian cells, NT-Ag-1.0 is better than PT in supporting epithelial cell viability. Proliferation of the seeded fibroblasts on NT-Ag-1.0 after 7 days is improved as well. After 1 day, the attached cells are observed by SEM and as shown in Fig. 6c–f, the epithelial cells adhere tightly to the substrates except NT-Ag-0.5 with dense filopodia. The cells on NT-Ag-1.0 even secrete abundant extracellular matrix to benefit cell proliferation. Fig. 6g, h, and j reveal that the fibroblasts on PT, NT, and NT-Ag-1.0 spread extensively and have a spindle shape. On the contrary, NT-Ag-0.5 is unfavorable to the spreading of fibroblasts for the adherent cells are still spherical in shape (Fig. 6i).

The gene expressions of cultured cells are sensitive to the underlying materials [30,31]. The change in cellular genes is objective and may take place earlier than other cellular alterations. The cells after culturing for 7 days are quantitatively determined by RT-PCR for genes of epithelial cells as VEGF (a glycoprotein inducing the microvascular permeability and angiogenesis during the wound healing stage) [32] and FN (a major component of serum and the periodontal tissues, playing an important role in the early wound healing events such as cells migration and adhesion) [33] and for genes of fibroblasts as Coll-I (the main component in gingival tissues which are associated with wound healing and peri-implant soft tissue sealing) [23,34] and ICAM-1 (an adhesion molecule belonging to the Ig super family, maintaining local host–parasite

Table 4
The green, red and total fluorescence intensities (Mean values ± SD) of Pg and Aa bacteria on various samples after culturing for 1 day. In the same column, values with different lowercase letter superscripts mean significant differences.

	P_g			A_a		
	Green	Red	Total	Green	Red	Total
PT	17.06 ± 1.99^a	0.21 ± 0.02^a	17.27 ± 2.02^a	18.11 ± 0.65^a	0.40 ± 0.02^a	18.51 ± 0.63^a
NT	27.78 ± 1.88^b	0.14 ± 0.01^a	27.92 ± 1.86^b	24.50 ± 2.13^b	0.50 ± 0.04^a	24.99 ± 2.17^b
NT-Ag-0.5	0.04 ± 0.01^c	7.08 ± 0.29^b	7.12 ± 0.27^c	0.02 ± 0.00^c	12.56 ± 0.94^b	12.57 ± 0.93^c
NT-Ag-1.0	0.08 ± 0.01^c	1.39 ± 0.02^c	1.47 ± 0.02^d	0.10 ± 0.02^c	3.93 ± 0.36^c	4.03 ± 0.34^d

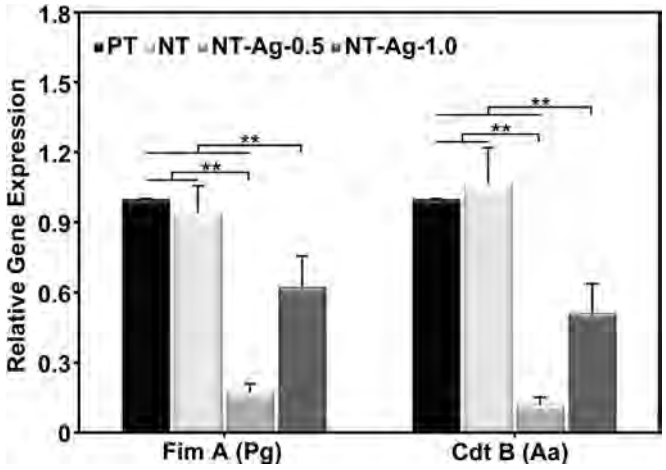

Fig. 4. RT-PCR analysis of selected genes for bacteria (Fim A for Pg, and Cdt B for Aa) after culturing on various samples for 1 day. One-way ANOVA followed by SNK *post hoc* test is utilized to determine the level of significance, $^{**}p < 0.01$.

equilibrium and limiting tissue damage *via* routing polymorphonuclear neutrophils to the gingival sulcus) [23,35]. The results are presented as histograms in Fig. 7a and b. Fig. 7a shows that NT and NT-Ag-1.0 up-regulate VEGF and FN expressions of the epithelial cells compared to PT and NT-Ag-0.5. The VEGF and FN levels on NT-Ag-0.5 are even lower than those on PT but the difference is not statistically significant ($p > 0.05$). Regarding the gene expressions of the incubated fibroblasts, the Coll-I level follows the order: NT > NT-Ag-1.0 > PT > NT-Ag-0.5 (Fig. 7b). Although the ICAM-1 expression on NT-Ag-1.0 is not as good as that on PT and NT, it is still much better than that on NT-Ag-0.5 and the difference is significant ($p < 0.01$).

In addition to *in vitro* tests, the samples are subjected *in vivo* assays to evaluate the foreign-body reactions. At 12 days after subcutaneous implantation into rats, the specimens with surrounding tissues are sectioned to determine the peri-implant conditions. Implants may elicit inflammatory responses in adjacent tissues leading to the formation of fibrotic capsules [36,37]. As shown by the hematoxylin and eosin staining results in Fig. 8a, the fibrotic capsule elicited by NT is significantly thinner than that induced by PT. This is strong evidence that the nanostructured

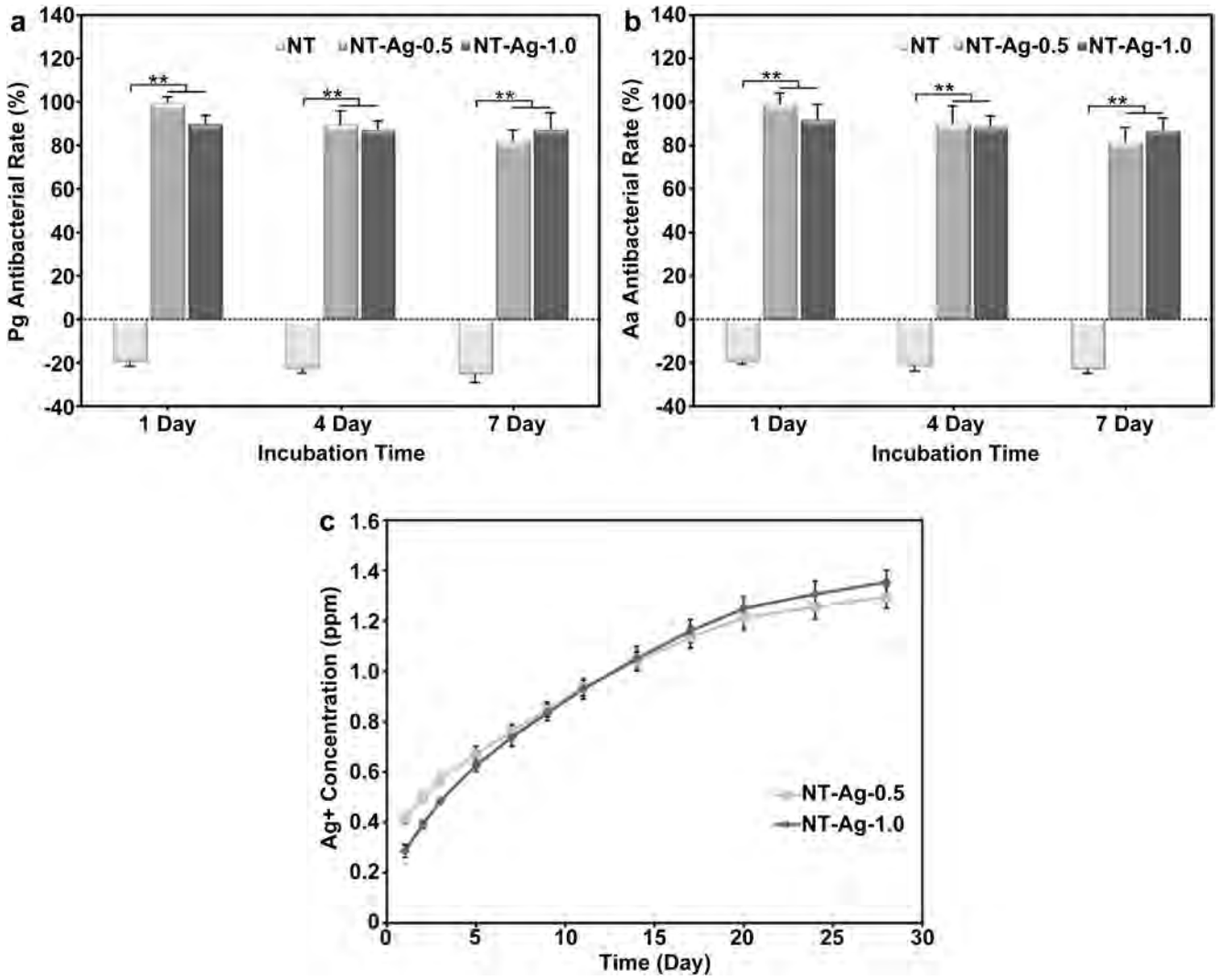

Fig. 5. Antibacterial effects and Ag release behaviors of various samples. (a,b) Time-dependent antibacterial rates of various samples against (a) Pg and (b) Aa up to 7 days, note that NT-Ag-0.5 and NT-Ag-1.0 are effective at sterilizing oral pathogens whereas NT is even more favorable to bacterial survival as compared to PT. One-way ANOVA followed by SNK *post hoc* test is utilized to determine the level of significance, $^{**}p < 0.01$. (c) Cumulative Ag release profiles from NT-Ag-0.5 and NT-Ag-1.0 by dynamic PBS immersion, note that NT-Ag-0.5 is better than NT-Ag-1.0 at early burst Ag release and NT-Ag-1.0 is more outstanding than NT-Ag-0.5 for sustained Ag delivery.

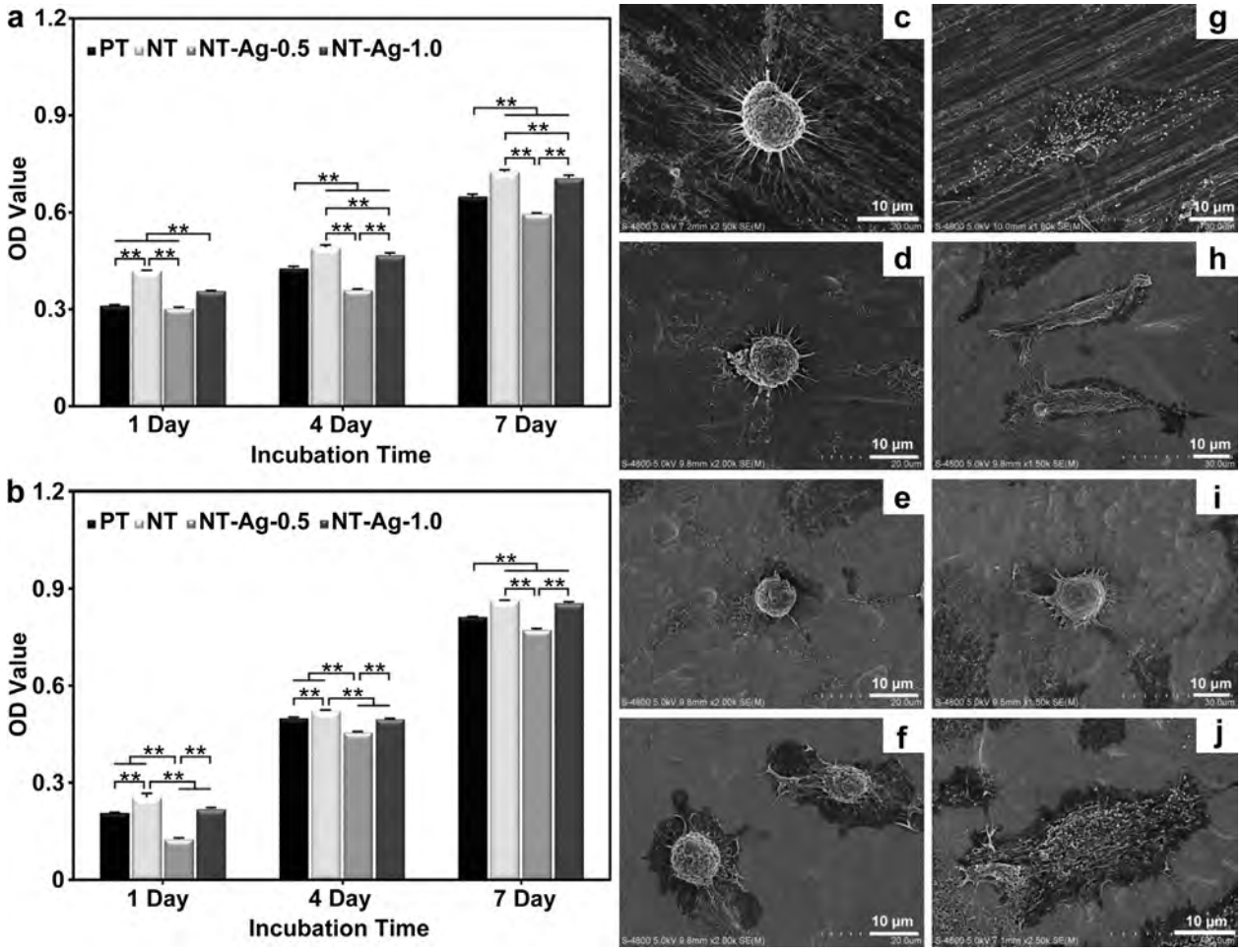

Fig. 6. Cell culture on the samples. (a, b) Time-dependent viabilities of (a) human epithelial cells and (b) fibroblasts on the samples up to 7 days. One-way ANOVA followed by SNK *post hoc* test is utilized to determine the level of significance, $^{**}p < 0.01$. (c–j) SEM observations of human epithelial cells (c–f) and fibroblasts (g–j) after culturing on PT (c, g), NT (d, h), NT-Ag-0.5 (e, i),m and NT-Ag-1.0 (f, j) for 1 day noting the difference in cellular morphologies between NT-Ag-0.5 and the other samples.

surface can lower the evoked tissue response such as capsule formation [37,38]. The reactive capsule thickness on NT-Ag-0.5 is higher compared to NT (Fig. 8a and c). Meanwhile, the fibrotic capsule elicited by NT-Ag-1.0 is slightly thinner than that on NT but without statistical significance ($p > 0.05$). The reactive capsules contain some inflammatory cells such as macrophages and the inflammatory cells are further assessed by immunofluorescence staining. The results reveal that the macrophages (cd68-positive cells) are abundant in the fibrotic capsules elicited by PT and NT-Ag-0.5 (Fig. 8b). On NT-Ag-0.5, the percentage of macrophages in relation to total cells is even higher than that on PT (Fig. 8c, $p < 0.05$), implying that the nanotubular sample with high-dose

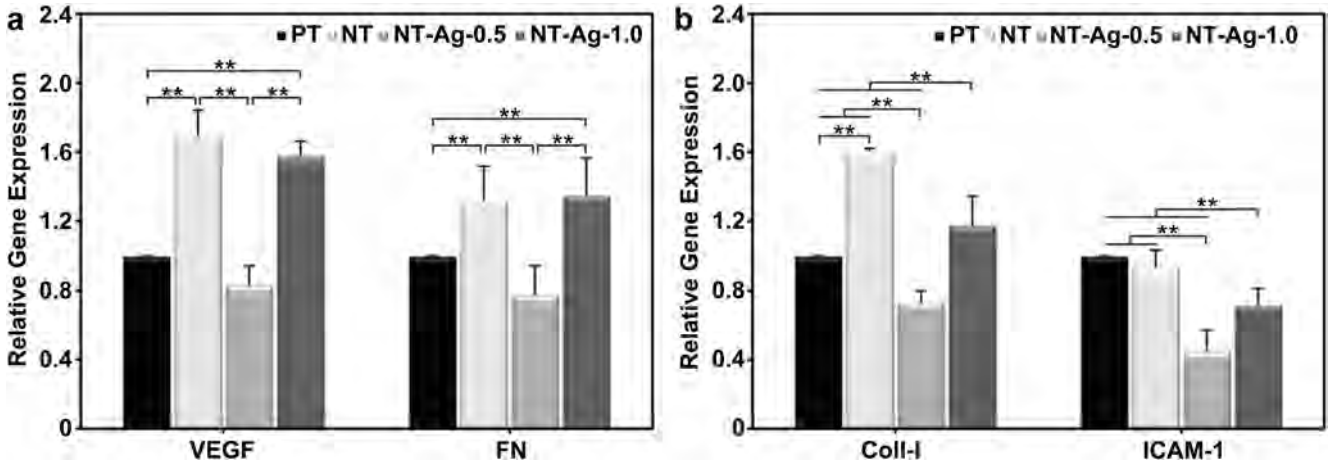

Fig. 7. RT-PCR analysis of (a) VEGF and FN for human epithelial cells and (b) Coll-I and ICAM-1 for fibroblasts after culturing on various samples for 7 days noting the down-regulations of all genes for cells on NT-Ag-0.5 with one-way ANOVA followed by SNK *post hoc* test utilized to determine the level of significance, $^{**}p < 0.01$.

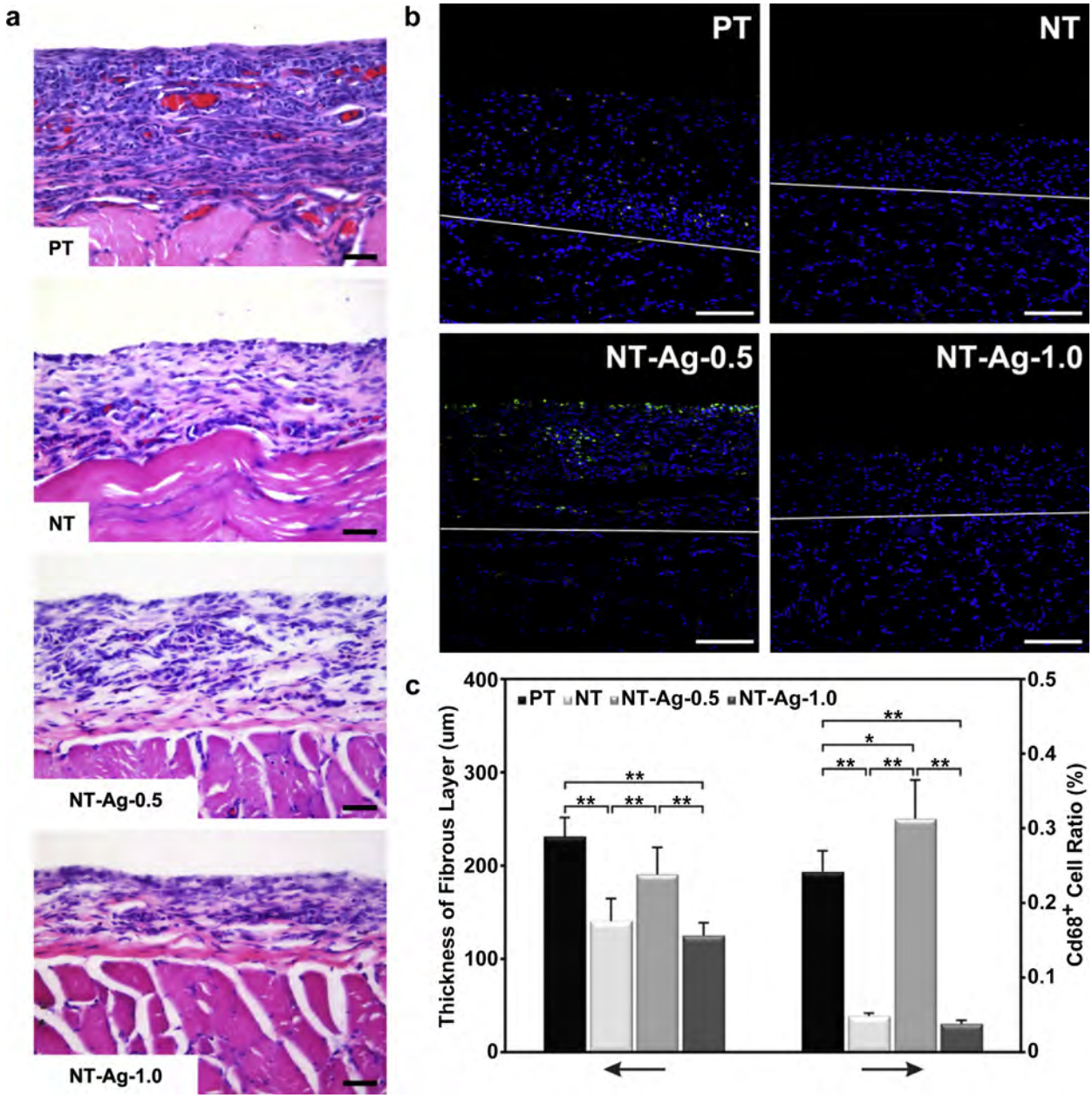

Fig. 8. *In vivo* biocompatibility of the samples: (a) Light micrographs of hematoxylin and eosin stained soft tissues previously in contact with the samples at 12 days post-implantation noting the difference in thickness for the fibrous capsules elicited by various samples. Scale bars for insets = 50 μm. (b) Confocal micrographs of cd68 positive cells and counterstained cells from soft tissues previously in contact with the samples at 12 days post-implantation noting the abundance of cd68 positive cells from soft tissues previously in contact with PT and NT-Ag-0.5. Scale bars for insets = 50 μm. (c) Thickness of fibrous capsules elicited and the ratio of cd68 positive cells recruited by various samples. One-way ANOVA followed by SNK *post hoc* test is utilized to determine the level of significance, $^{*}p < 0.05$, $^{**}p < 0.01$.

superficial Ag is more inflammatory than PT *in vivo*. In contrast, the cd68-positive cells recruited by NT and NT-Ag-1.0 are rare in the much thinner fibrotic capsules (Fig. 8b). These morphometry and immunohistochemistry results demonstrate that NT and NT-Ag-1.0 are much more acceptable than PT and NT-Ag-0.5 *in vivo*.

4. Discussion

In modern dentistry, dental implants made of Ti are widely used to treat edentulous patients [39,40] due to the excellent osseointegration with jaw bones. Nonetheless, infection prevention is a continuous challenge as pathogens are abundant in the oral environment and Ti is non-antibacterial inherently. All the dental implants today are root-form endosseous implants but parts of them (trans-gingival parts) are beyond the jaw bones in contact with epithelial and fibrous tissues. In this respect, integration between the trans-gingival parts and connective soft tissues is essential to the formation of peri-implant soft tissue seals. A healthy and tight peri-implant soft tissue seal is of prime importance since it can serve as the protective barrier to prevent implants from mechanical damage and microbial invasion. Biomaterials are artificial or natural materials made into specific structures to replace lost or diseased biological structures in order to restore biofunctions. With regard to the higher expectation of life quality and human longevity, the advancement of biomaterials is imperative and the related studies are growing fast. Specific to Ti dental

implants, endowing the trans-gingival parts with the proper antibacterial ability as well as better compatibility with soft tissues is desirable. To attain this goal, anodization and Ag PIII are proposed and described here.

Anodization is a convenient technique to fabricate TiO_2-NTs on Ti and the size of the TiO_2-NTs can be varied from tens to hundreds of nanometers by adjusting the parameters [20–22]. Here, the TiO_2-NTs with a diameter of 80 nm have excellent properties *in vitro* and exhibit less inflammatory responses *in vivo*. To enhance the antibacterial capability, Ag PIII is performed after anodization. By adopting the suitable PIII instrumental parameters, the TiO_2-NTs retain the nanoscale morphology and are doped with Ag at different sites and depths. Both Ag PIII samples (NT-Ag-0.5 and NT-Ag-1.0) are effective in sterilizing oral pathogens and the latter sample shows a better Ag leaching profile due to the deeper distribution. NT-Ag-0.5 and NT-Ag-1.0 also vary in other bio-functions as NT-Ag-1.0 has less surface Ag accumulation and a large amount of surface Ag can be detrimental to cells and soft tissues. NT-Ag-1.0 is more favorable to epithelial cells and fibroblasts *in vitro* and *in vivo*. The thinner fibrotic capsule elicited by NT-Ag-1.0 is less inflammatory compared to NT-Ag-0.5. As a new type of surface-modified Ti nanostructures, NT-Ag-1.0 combines excellent antibacterial ability and biocompatibility and has large potential in dental implants.

5. Conclusion

Nanotubular structures are fabricated on Ti plates by anodization and ensuing Ag PIII under optimal conditions produces excellent antibacterial effects and biocompatibility both *in vitro* and *in vivo*. Unlike conventional chemical techniques which introduce the largest amount of Ag to the near surface, the concentration and depth of the embedded Ag can be altered readily by adjusting the PIII parameters to attain the optimal performance. NT-Ag-0.5 shows a larger burst of Ag release in the beginning but NT-Ag-1.0 produces better and more sustained Ag delivery. NT-Ag-0.5 is more antimicrobial than NT-Ag-1.0 in the early stage, but NT-Ag-1.0 outperforms NT-Ag-0.5 in sustained antibacterial experiments. Although NT-Ag-0.5 can inactivate oral pathogens, its *in vitro* and *in vivo* biocompatibility is impaired by the large amount of surface Ag. On the other hand, NT-Ag-1.0 is as good as NT in terms of functionalization of epithelial cells and fibroblasts *in vitro* and elicits less inflammatory responses *in vivo*. NT-Ag-1.0 is thus very attractive in trans-gingival abutment of dental implants.

Acknowledgments

The authors acknowledge financial support from National Natural Science Foundation of China (Nos. 81070862, 81201203, 31170915 and 31200716), Hong Kong Research Grants Council General Research Funds (Nos. 112510 and 112212), City University of Hong Kong Applied Research Grants (Nos. 9667066 and 9667069), as well as the Shenzhen Peacock Program (No. 110811003586331).

References

[1] Geetha M, Singh AK, Asokamani R, Gogia AK. Ti based biomaterials, the ultimate choice for orthopaedic implants–a review. Prog Mater Sci 2009;54:397–425.
[2] Niinomi M. Mechanical biocompatibilities of titanium alloys for biomedical applications. J Mech Behav Biomed 2008;1:30–42.
[3] Puleo DA, Kissling RA, Sheu MS. A technique to immobilize bioactive proteins, including bone morphogenetic protein-4 (BMP-4), on titanium alloy. Biomaterials 2002;23:2079–87.
[4] Cioffi M, Gilliland D, Ceccone G, Chiesa R, Cigada A. Electrochemical release testing of nickel-titanium orthodontic wires in artificial saliva using thin layer activation. Acta Biomater 2005;1:717–24.
[5] Long M, Rack HJ. Titanium alloys in total joint replacement–a materials science perspective. Biomaterials 1998;19:1621–39.
[6] Hardes J, Ahrens H, Gebert C, Streitbuerger A, Buerger H, Erren M, et al. Lack of toxicological side-effects in silver-coated megaprostheses in humans. Biomaterials 2007;28:2869–75.
[7] Zhao LZ, Wang HR, Huo KF, Cui LY, Zhang WR, Ni HW, et al. Antibacterial nano-structured titania coating incorporated with silver nanoparticles. Biomaterials 2011;32:5706–16.
[8] Zheng YH, Li JB, Liu XY, Sun J. Antimicrobial and osteogenic effect of Ag-implanted titanium with a nanostructured surface. Int J Nanomedicine 2012;7:875–84.
[9] Goodman SB, Yao ZY, Keeney M, Yang F. The future of biologic coatings for orthopaedic implants. Biomaterials 2013;34:3174–83.
[10] Zhao LZ, Chu PK, Zhang YM, Wu ZF. Antibacterial coatings on titanium implants. J Biomed Mater Res B 2009;91B:470–80.
[11] Harris LG, Tosatti S, Wieland M, Textor M, Richards RG. Staphylococcus aureus adhesion to titanium oxide surfaces coated with non-functionalized and peptide-functionalized poly(L-lysine)-grafted-poly(ethylene glycol) copolymers. Biomaterials 2004;25:4135–48.
[12] Kingshott P, Wei J, Bagge-Ravn D, Gadegaard N, Gram L. Covalent attachment of poly(ethylene glycol) to surfaces, critical for reducing bacterial adhesion. Langmuir 2003;19:6912–21.
[13] Necula BS, Fratila-Apachitei LE, Zaat SA, Apachitei JI, Duszczyk J. In vitro antibacterial activity of porous TiO_2-Ag composite layers against methicillin-resistant staphylococcus aureus. Acta Biomater 2009;5:3573–80.
[14] Agarwal A, Weis TL, Schurr MJ, Faith NG, Czuprynski CJ, McAnulty JF, et al. Surfaces modified with nanometer-thick silver-impregnated polymeric films that kill bacteria but support growth of mammalian cells. Biomaterials 2010;31:680–90.
[15] Agarwal A, Guthrie KM, Czuprynski CJ, Schurr MJ, McAnulty JF, Murphy CJ, et al. Polymeric multilayers that contain silver nanoparticles can be stamped onto biological tissues to provide antibacterial activity. Adv Funct Mater 2011;21:1863–73.
[16] Cao HL, Liu XY, Meng FH, Chu PK. Biological actions of silver nanoparticles embedded in titanium controlled by micro-galvanic effects. Biomaterials 2011;32:693–705.
[17] Greulich C, Braun D, Peetsch A, Diendorf J, Siebers B, Epple M, et al. The toxic effect of silver ions and silver nanoparticles towards bacteria and human cells occurs in the same concentration range. RSC Adv 2012;2:6981–7.
[18] Chernousova S, Epple M. Silver as antibacterial agent: ion, nanoparticle, and metal. Angew Chem Int Ed 2013;52:1636–53.
[19] Crawford GA, Chawla N, Das K, Bose S, Bandyopadhyay A. Microstructure and deformation behavior of biocompatible TiO_2 nanotubes on titanium substrate. Acta Biomater 2007;3:359–67.
[20] Park J, Bauer S, von der Mark K, Schmuki P. Nanosize and vitality: TiO_2 nanotube diameter directs cell fate. Nano Lett 2007;7:1686–91.
[21] Park J, Bauer S, Schlegel KA, Neukam FW, von der Mark K, Schmuki P. TiO_2 nanotube surfaces: 15 nm–an optimal length scale of surface topography for cell adhesion and differentiation. Small 2009;5:666–71.
[22] Oh S, Brammer KS, Li YSJ, Teng D, Engler AJ, Chien S, et al. Stem cell fate dictated solely by altered nanotube dimension. Proc Natl Acad Sci U S A 2009;106:2130–5.
[23] Ma QL, Mei SL, Ji K, Zhang YM, Chu PK. Immobilization of Ag nanoparticles/FGF-2 on a modified titanium implant surface and improved human gingival fibroblasts behavior. J Biomed Mater Res A 2011;98A:274–86.
[24] Mei SL, Zhao LZ, Wang W, Ma QL, Zhang YM. Biomimetic titanium alloy with sparsely distributed nanotubes could enhance osteoblast functions. Adv Eng Mater 2012;14:166–74.
[25] Shibata Y, Suzuki D, Omori S, Tanaka R, Murakami A, Kataoka Y, et al. The characteristics of in vitro biological activity of titanium surfaces anodically oxidized in chloride solutions. Biomaterials 2010;31:8546–55.
[26] Pritchard EM, Valentin T, Panilaitis B, Omenetto F, Kaplan DL. Antibiotic-releasing silk biomaterials for infection prevention and treatment. Adv Funct Mater 2013;23:854–61.
[27] Zilberman M, Elsner JJ. Antibiotic-eluting medical devices for various applications. J Control Release 2008;130:202–15.
[28] Yoshimura F, Murakami Y, Nishikawa K, Hasegawa Y, Kawaminami S. Surface components of *Porphyromonas gingivalis*. J Periodontal Res 2009;44:1–12.
[29] Mayer MPA, Bueno LC, Hansen EJ, DiRienzo JM. Identification of a cytolethal distending toxin gene locus and features of a virulence-associated region in *Actinobacillus actinomycetemcomitans*. Infect Immun 1999;67:1227–37.
[30] Wang HY, Kwok DTK, Wang W, Wu ZW, Tong LP, Zhang YM, et al. Osteoblast behavior on polytetrafluoroethylene modified by long pulse, high frequency oxygen plasma immersion ion implantation. Biomaterials 2010;31:413–9.
[31] Wang HY, Kwok DTK, Xu M, Shi HG, Wu ZW, Zhang W, et al. Tailoring of mesenchymal stem cells behavior on plasma-modified polytetrafluoroethylene. Adv Mater 2012;24:3315–24.
[32] Schultze-Mosgau S, Wehrhan F, Wichmann M, Schlegel KA, Holst S, Thorwarth M. Expression of interleukin 1-beta, transforming growth factor beta-1, and vascular endothelial growth factor in soft tissue over the implant before uncovering. Oral Surg Oral Med Oral Pathol Oral Radiol Endod 2006;101:565–71.

[33] Jones RA, Nicholas B, Mian S, Davies PJA, Griffin M. Reduced expression of tissue transglutaminase in a human endothelial cell line leads to changes in cell spreading, cell adhesion and reduced polymerisation of fibronectin. J Cell Sci 1997;110:2461–72.
[34] Shioya K, Sawada T, Miake Y, Inoue S, Yanagisawa T. Ultrastructural study of tissues surrounding replanted teeth and dental implants. Clin Oral Implants Res 2009;20:299–305.
[35] Tonetti MS, Imboden MA, Lang NP. Neutrophil migration into the gingival sulcus is associated with transepithelial gradients of interleukin-8 and ICAM-1. J Periodontol 1998;69:1139–47.
[36] Remes A, Williams DF. Immune-response in biocompatibility. Biomaterials 1992;13:731–43.
[37] Linsmeier CE, Wallman L, Faxius L, Schouenborg J, Bjursten LM, Danielsen N. Soft tissue reactions evoked by implanted gallium phosphide. Biomaterials 2008;29:4598–604.
[38] Rosengren A, Wallman L, Danielsen N, Laurell T, Bjursten LM. Tissue reactions evoked by porous and plane surfaces made out of silicon and titanium. IEEE Trans Bio-Med Eng 2002;49:392–9.
[39] Arvidson K, Bystedt H, Frykholm A, von Konow L, Lothigius E. Five-year prospective follow-up report of the Astra Tech Dental Implant System in the treatment of edentulous mandibles. Clin Oral Implants Res 1998;9:225–34.
[40] Astrand P, Ahlqvist J, Gunne J, Nilson H. Implant treatment of patients with edentulous jaws: a 20-year follow-up. Clin Implant Dent Res 2008;10:207–17.